Nanoscale Advances

Accepted Manuscript

This article can be cited before page numbers have been issued, to do this please use: M. Toma and K. Tawa, *Nanoscale Adv.*, 2019, DOI: 10.1039/C9NA00315K.

ROYAL SOCIETY OF CHEMISTRY

rsc.li/nanoscale-advances

View Article Online
DOI: 10.1039/C9NA00315K

ARTICLE

Plasmonic Coloration of Silver Nanodome Arrays for Smartphone-based Plasmonic Biosensor

Received 00th January 20xx,
Accepted 00th January 20xx

DOI: 10.1039/x0xx00000x

Mana Toma,*[a, †] and Keiko Tawa [a]

In this study, the utility of plasmonic coloration on silver nanodome arrays for sensitive and quantitative detection of biomolecules by a smartphone-based measurement is proposed. Particularly a quantitative analysis of DNA hybridization was achieved using hue angle in HSV color space obtained from a photograph of sensing spot taken by a smartphone camera. Silver and gold nanodome arrays consisting of polystyrene beads layer covered with a thin metal film can be created over the large area by a bottom-up fabrication process. The metal nanodome arrays exhibited unique colorations which can be tuned by the dome diameter ϕ, metal species, and the refractive index of surrounding medium. The measurement of bulk refractive index sensitivity revealed that the Ag nanodome (ϕ=500 nm) can provide the highest sensitivity up to 588 nm per refractive index unit. Detection of DNA hybridization was performed by using bimetallic nanodome consisting of silver and thin gold overlayer, and DNA modified gold nanoparticles (AuNPs) for enhancing the sensor signals. Upon the immobilization of AuNPs, the Ag nanodome (ϕ=200 nm) exhibited a large shift in resonance wavelength accompanied with the dramatic change in coloration. The analysis of detection sensitivity of DNA hybridization using a model system revealed that the colorimetric detection based on hue can be used for quantitative detection of biomolecules in the same manner as spectroscopic method with few pM level detectable concentration.

Introduction

In the last three decades, surface plasmon biosensors have become an established analytical tool for biomolecular interactions and sensitive detection of various biomolecules.[1-5] Due to the growth of demands on detection methods of target molecules relating to point of care testing and environmental monitoring, establishment of a portable plasmonic biosensors has emerged as one of the important subjects.[6-11] To miniaturize plasmonic biosensors, implementation of metal nanostructures is a straightforward approach as the resonance condition of surface plasmon are highly controllable by the geometry of metal layer. For instance, diffraction gratings coated with a thin metal film have been employed to utilize the nature of propagating surface plasmon called grating coupled surface plasmon resonances (GC-SPR) without using a prism.[10-13] Along with GC-SPR, localized surface plasmon resonances (LSPR) on metal nanostructures have been widely used for biosensor applications.[3, 14] Recent progress of plasmonic metamaterials consisting of two or three dimensional metal nanostructure arrays has been providing ways to design high performance plasmonic biosensors.[15, 16] Initially, the miniaturization of plasmonic biosensor have been achieved by simplifying the optical setup. Nowadays, development of smartphone-based plasmonic biosensors is attracting great attentions as optical measurement can be performed with the light source and digital cameras integrated in a smartphone by using the proper attachment.[7, 11, 17, 18] For example, biomolecular detection was performed by smartphone-based surface plasmon resonance imaging using a sensor chip supporting GC-SPR, and detection of mouse IgG at nM level was demonstrated.[18] Likewise the conventional plasmonic biosensors, various optical signals can be recorded by a smartphone-based sensing system, such as reflectance and transmittance at a fixed wavelength or spectroscopic readout. Colorimetric detection is one of the attractive methods, which can be unique for smartphone-based plasmonic biosensor. [7] In a colorimetric plasmonic biosensor, immobilization of target molecules onto the sensor surface can be detected as change in coloration of sensing spot, quantified by measurement of changes in RGB values or shift in Hue angles in a color space obtained from photographs. Therefore, a camera function of smartphone can be used as it is without using the additional attachment for spectroscopic measurement. Though the idea of colorimetric detection has been adopted in the plasmonic biosensors utilizing aggregation of metal nanoparticles in aqueous solution,[19, 20] spectroscopic measurement and visual examination are commonly combined for biosensing. On this point, plasmonic coloration from metal nanostructure arrays created on the solid substrate may hold potential for

[a] Department of Applied Chemistry for Environment, School of Science and Technology, Kwansei Gakuin University, Sanda, Japan 669-1337.
† Present address: Department of Electrical and Electronic Engineering, School of Engineering, Tokyo Institute Technology, Yokohama, Japan 226-5919 E-mail: toma.m.aa@m.titech.ac.jp.
Electronic Supplementary Information (ESI) available: The schematic drawing of the surface modification process of sensor surface, UV-Vis absorption spectra of DNA modified AuNPs; sketch of optical setup; Photographs of Ag nanodome arrays (ϕ=350 nm) created with various Ag thickness; Transmission spectra of Ag nanodome arrays taken at various incident angles; a video of reversible change on coloration of Ag nanodome arrays. See DOI: 10.1039/x0xx00000x

quantitative analysis by RGB values or color space coordinates, as well as the easiness of implementation into a lab-on a chip device. The color generation of metal nanostructure arrays have been widely studied for plasmonic color printing technology,[21-24] and up to now, several research groups have reported the possibility of the plasmonic coloration of metal nanostructure arrays for colorimetric biosensor applications.[7, 25-27] Shinohara *et al.* had reported the dramatic change in the coloration of the silver nanoparticle sheet due to immobilization of gold nanoparticles via biotin-avidin interaction.[25] Recently, the detection of streptavidin at sub nM level had been reported by using gold-silver alloy nanodisk arrays.[27] Nevertheless, the reports on colorimetric plasmonic biosensor based on metal nanostructure arrays mainly demonstrated bulk refractive index measurement or detection of biomolecules at high concentration range. Furthermore, most of colorimetric detection schemes reported the changes of colors in photographs and actual quantitative analysis were performed by spectroscopic methods.

Herein, we report the colorimetric plasmonic biosensor scheme which can perform quantitative analysis of biomolecules by measuring hue angle in HSV (hue, saturation and value) color space obtained from RGB value of photograph. Our metal nanodome arrays consists of metal coated polystyrene (PS) beads layer which is also referred to as metal semi-shells or metal half sells structures.[28-30] The metal nanodome arrays are considered to be an attractive plasmonic metamaterials, as the structures can be created over the large area (centimeter scale) by a simple and scalable bottom-up nanofabrication process, and their optical properties are controllable by the size of PS beads and component of metal layer. In this study, we created the metal nanodome arrays by using PS beads with diameters ϕ of 200, 350 and 500 nm and metal thin films, namely silver and gold. The fundamental optical properties and sensing performance of metal nanodome array were investigated by spectroscopic method as well as colorimetric method based on the image analysis of photograph. Specifically, the optical properties of metal nanodome arrays were investigated by reflectivity measurements, and their plasmonic colorations were evaluated by using Hue, saturation and value (HSV) coordinate in a color space. Then, the bulk refractive index measurement was carried out by spectroscopic measurement to investigated the fundamental sensing properties of metal nanodome arrays. For a biosensor application, detection of DNA hybridization was performed by using a bimetallic layer structure by coating the surface of Ag nanodome with a thin Au over layer (ca. 6 nm thick) to prevent oxidization of Ag layer. In addition, DNA modified gold nanoparticles (AuNPs) was used to enhance the sensor signals. The sensor signals induced by the immobilization of DNA-AuNPs via DNA hybridization were compared among the Ag nanodome arrays with different dome size. The detailed characterization of sensing performance was carried out by using Ag nanodome arrays (ϕ= 200 nm) which exhibited the largest shift in resonance wavelength upon the binding of DNA-AuNPs, accompanied with dramatic changes in the coloration of sensing spot. Furthermore, quantitative measurement of sensor signals defined by the shift in resonance wavelength as well as Hue angles were demonstrated to evaluate the performance characteristics of colorimetric plasmonic biosensor utilizing Ag nanodome array structures including detection sensitivity.

Experimental

Materials.

Carboxylate-coated polystyrene (PS) beads solutions (2.6 % w/v, 200, 350 and 500 nm in diameter (ϕ) were obtained from Polysciences. Dopamine hydrochloride, ethylene glycol, Gold(III) chloride hydrate, TritonX and Phosphate buffered saline tablets were purchased from Sigma. Trisodium Citrate was obtained from Wako Pure Chemical Co. Three single-stranded DNA (ssDNA) sequences were purchased from Integrated DNA Technologies. The sequences are denoted Rc30, R30, and T30: Rc30 = 5′-NH2(CH2)12CGAAATCCAGACACATAAGCACGAACCGAA-3′, R30 = 5′-SH-$(CH_2)_6$-TTCGGTTCGTGCTTATGTGTCTGGATTTCG-3′, and T30 = 5′-NH_2-(CH2)12-(T)30-3′. All the chemicals were used as received.

Fabrication of metal nanodome arrays.

The Ag nanodome array structures were fabricated by a simple and scalable process as shown in Figure 1a. Firstly, the PS beads solution was spin coated onto the cleaned glass substrate as described elsewhere.[31, 32] The solvent of PS beads solution was replaced with the mixed solvent of water and ethanol with a mixing volume ratio of 1 : 3. In an ethanol solution, a spike of Triton X was added to 0.2 v% as a surfactant. The concentration of PS beads solution was adjusted to roughly from 1 w% to 2.5 w% for 200 to 500 nm PS beads, respectively. For spincoating process, a typical condition (1,000 rpm for 6 sec) was used. The substrate was placed in a plastic petri-dish in order to let the solvent dry slowly and PS beads form closely packed layers by self-assembly process. Ag or Au thin films were deposited by Rf sputtering. The thin Ti layer was used as an adhesion layer of Ag thin film. The Ag thickness was varied from 30 to 130 nm, but the typical Ag thickness was 53±1 nm. Before conducting experiments, the substrates were annealed at 100 °C on a hotplate for a couple of minutes to improve the adhesion of PS beads onto the glass substrate. For biosensor application, the patterned sensing spots were created by using a stencil mask made from a Kapton tape. The diameter of each sensing spot is about 2 mm and seven spots were created on one sensor chip.

Sensor surface functionalization.

The sensor surface was modified with a single stranded DNA for the detection of DNA hybridization. The surface modification process was described in Figure S1 in the supporting information. For biosensor application, an additional Au layer (thickness: 6 ± 1 nm) was sputtered on top of the Ag nanodome arrays to prevent oxidation of Ag layer in aqueous environment. The polydopamine chemistry was employed to anchor the amino-terminated single stranded DNA as described elsewhere.[33] After annealing the substrate, a solution of dopamine hydrochloride adjusted to 2 mg/mL in a Tris buffer (10 mM, pH 8.5) was dropped on the sensor surface. After 10 min incubation, the sensor surface was rinsed with MilliQ water,

View Article Online
DOI: 10.1039/C9NA00315K

and dried with a N_2 stream. The amino-terminated ssDNA solution adjusted to 250 μM in PBS was applied onto the sensor spot, then incubated overnight. The sensor surface was rinsed with PBS buffer before measurement.

Synthesis of gold nanoparticles.

AuNPs with a diameter of around 15 nm were synthesized by citrate reduction. Briefly, $HAuCl_4$ was dissolved in water (0.26 mM, 19 mL), and sodium citrate dihydrate (20 mM, 1 mL) was then injected to the boiling solution. After a, the reaction solution was continued to boil, until the color of the solution turned red. The AuNPs solution was purified by centrifuge separation for three times, then stored after re-dispersion in MilliQ water. The ligand exchange of the AuNPs was described in the previous paper.[34] The concentration of AuNPs was set to ca. 3 nM by UV-vis absorption spectra using the molar extinction coefficient of 2.7 x 10^8 $M^{-1}cm^{-1}$.[33] The UV-vis absorption spectrum was shown in Figure S2 in the supporting information. As shown in Fig. S2, the DNA-AuNPs showed the absorption peak induced by LSPR at 525 nm.

Optical Setup.

A laboratory-build optical setup was used for the reflectivity measurement as shown in Figure S3 in the supporting information. A white right from a tungsten halogen lamp (SLS201/M, Thorlabs) was coupled into a fiber optics (M92L01, 200 μm, 0.22NA, Thorlabs), and collimated by using a collimation mirror (RC08SMA-P01, Thorlabs). A collimated beam passed a beam splitter (PDBSH-25.4C1.5, Sigma-Koki), and focused on the sensor surface by a concave lens (SL-SQ-25-150P, Sigma-Koki). The spot size on the sample surface was about 1 mm in diameter. A sensor chip was set to a rotation stage (SGSP-60YAW-0B, Sigma-Koki) to adjust the incident angle to zero degree. A sensor chip covered with Ag nanodome arrays was fixed to a holder, which was attached to helicoidal post holder and linear stage to adjust the position of sensing spot. To conduct an experiment in aqueous solution, a flow cell made from PDMS sheet was placed on the surface of sensor chip. The sample solution was introduced by an injection syringe, or flowed over the sensor surface by a peristaltic pump. The reflected light was partially reflected by the beam splitter and coupled into a fiber optics by using a condenser lens (F810SMA-635, Thorlabs) connected to a spectrometer (Maya2000, Ocean Optics). Spectrometer control, data acquisition as well as data analysis was performed by LabVIEW software. An Al mirror (TFA-20C03-10, Sigma-Koki) was used to obtain a reference spectrum. The reflectivity spectra were fitted with a quadratic equation by using the threshold value to determine the reflectivity minimum.

Hue angle measurement.

The photograph of Ag nanodome array was taken by a smartphone camera (Nexus, LG) under the illumination of fluorescent lamp. The automatic function was selected to adjust the white balance and brightness. The RGB value of the sensor spot was obtained from the photograph by using ImageJ (US National Institutes of Health, http://imagej.nih. gov/ij/) and a function called color histogram. Then, the hue (H), saturation (S) and value (V) were calculated from the RGB values using the algorithm described in the literature.[31]

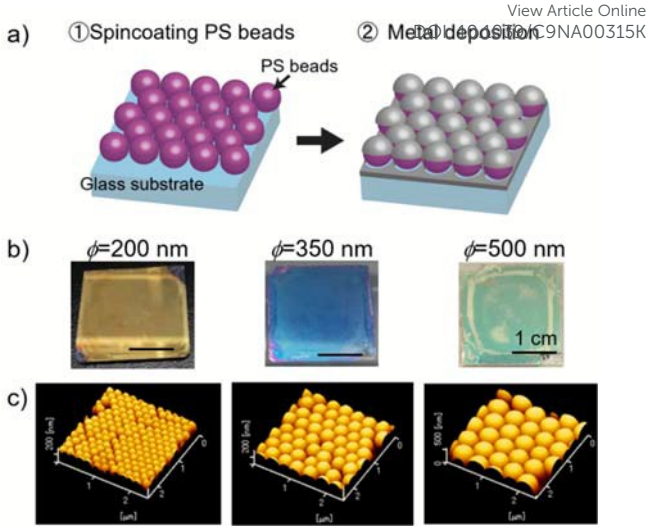

Figure 1 (a) Schematic drawing of the fabrication process, (b) representative photographs and (c) AFM images of Ag nanodome arrays (left: ϕ= 200 nm, middle: ϕ= 350 nm, right: ϕ= 500 nm).

Results and discussion

Characterization of Ag nanodome arrays.

When the PS beads layers were coated with Ag thin film, the Ag nanodome surface exhibited unique coloration depending on the size of PS beads ϕ. Figure 1b shows the typical photographs of Ag nanodome arrays created with 50 nm thick Ag layer. The Ag nanodome array structures were created over the area of glass slide cut into 2.5 × 2.5 cm^2 indicated as the generation of plasmonic coloration. Ag nanodome arrays exhibited gold (ϕ= 200 nm) and blue (ϕ= 350 nm). As the size of nanodome enlarged (ϕ= 500 nm), it showed coloration changing by the viewing angles, indicating the nature of iridescence due to the diffraction. When the thickness of Ag layer was varied, the appearance of Ag nanodome arrays dramatically changed. The photographs of Ag nanodome arrays (ϕ= 350 nm) with various Ag thickness are shown in Figure S4 in the supporting information. As shown in photographs, the thinner Ag layer with a thickness of 30 nm resulted in the increase of transparency. On the other hand, the coloration faded by increasing the thickness of Ag layer more than 100 nm. From these observations, we consider that the optimum thickness of Ag layer to generate vivid coloration is in the range from 40 to 60 nm. Atomic force microscope (AFM) observation was performed to characterize the structure of Ag nanodome arrays. Figure 1c shows the representative AFM images of the Ag nanodome arrays created with different size of PS beads (ϕ= 200, 350 and 500 nm). From these AFM images, formations of the closely-packed PS beads layer were confirmed. The fundamental optical properties of the Ag nanodome arrays were investigated by reflectivity measurement at vertical incidence. Figures 2a-d show the reflectivity spectra and the

View Article Online
DOI: 10.1039/C9NA00345K

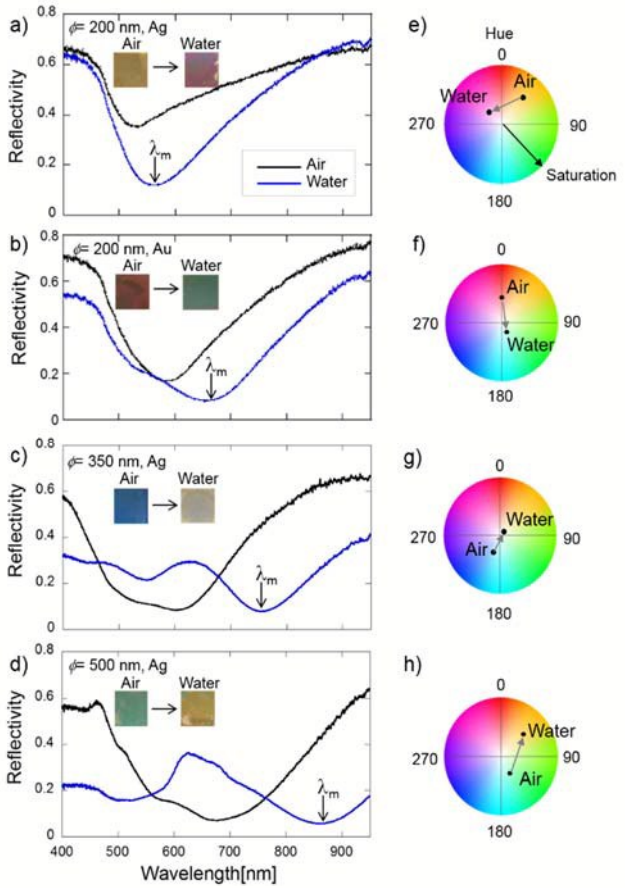

Figure 2 Reflectivity spectra and photograph of Ag and Au nanodome arrays taken in air and water (left column), and coloration scale (right column). Metal species and size of PS beads are a) and e) Ag (ϕ= 200 nm), b) and f) Au (ϕ= 200 nm), c) and g) Ag (ϕ= 350 nm), d) and h) Ag (ϕ= 500 nm).

Table 1 Summary on resonance wavelengths and HSV coordinates in color space of metal nanodome array

ϕ [nm]	Metal	λ_m [nm]		HSV coordinate	
		in air	in water	in air	in water
200	Ag	532	560	(40, 0.56, 0.79)	(314, 0.28, 0.59)
200	Au	586	650	(2, 0.43, 0.69)	(150, 0.21, 0.44)
350	Ag	617	785	(201, 0.30, 0.55)	(43, 0.10, 0.63)
500	Ag	677	850	(147, 0.31, 0.55)	(42, 0.57, 0.50)

photograph of Ag and Au nanodome arrays in contact with air and water. The reflectivity spectra of each metal nanodome arrays exhibited reflectivity drops associated with resonant excitation of surface plasmon, which are varied by the size of nanodome. The red shift of resonance wavelength λ_m of main dip occurred as the size of Ag nanodome increased, which is in good agreement to the literature.[29, 36] The resonance curves of Ag nanodome array (ϕ= 350 and 500 nm) exhibited two dips, indicating that these metal nanodome array structures hold multiple optical modes. The appearance of additional features in shorter wavelength region was likely due to the far field diffraction and photonic mode of PS beads.[36] The Au nanodome arrays (ϕ= 200 nm) exhibited the resonance at longer wavelength with respect to the Ag nanodome arrays with the same dome diameter, and exhibited red color in air. When a water droplet was applied on top of the metal nanodome array surface, the deformation of reflectivity spectra occurred accompanied with the dramatic color change. The deformation of reflectivity spectra was dominantly due to the red shift of resonance wavelength λ_m caused by the increase of refractive index of surrounding medium from air to water. The resonance wavelength λ_m of main dip and hue, saturation and value (HSV) coordinates in a color space are summarized in Table 1. The saturation and value are defined in the range from 0 to 1. Let us note that chroma and brightness are correlated to saturation and value, respectively.

The Ag nanodome array (ϕ= 200 nm) exhibited the smallest shift in resonance wavelength λ_m ca. 30 nm from air to water in the reflectivity measurement. On the other hand, the coloration dramatically changed from yellow to red along with the shift of Hue angels in counterclockwise direction from 40 to 314 deg (ΔHue=86 deg). In the case of Au nanodome array (ϕ= 200 nm), the shift in the resonance wavelength resulted in 64 nm, and the shift in Hue reached to about 150 deg. The shift of resonance wavelength λ_m increased to 168 nm for the Ag nanodome array (ϕ= 350 nm). However, the bluish color in air faded by applying a water drop, indicated by the decrease of saturation from 0.3 to 0.1 as well. We consider this is the result of shift of resonance wavelength to the near infrared wavelength region which leaded to flatten the reflectivity spectra in the visible wavelength region. The largest Ag nanodome array (ϕ= 500 nm) exhibited shift in the resonance wavelength as high as 173 nm, the color turned from light green to yellow with shift in Hue angle as 105 deg. Nevertheless, the coloration can be changed by the viewing angle. The angular dependent optical properties of Ag nanodome arrays were observed by the transmission spectra taken at various incident angles. As shown in figures S5 in the supporting information, the peak wavelength shifted as the incident angle increased for the large Ag nanodome arrays (ϕ= 500 nm). As the size of nanodome decreased, the peak shift was not significant. Based on the spectroscopic measurements, the larger Ag nanodome arrays exhibited higher responses as shifts in resonance wavelength. On the other hand, Ag and Au nanodome arrays (ϕ= 200 nm) exhibited vivid coloration both in air and aqueous environment, indicating their potentials for colorimetric detection.

The change in coloration of metal nanodome arrays caused by the increase of refractive index of surrounding medium quickly occurred, and was reversible. A video in the supporting information shows the coloration of Ag nanodome arrays (ϕ= 200 nm) immediately changed from yellow to purple when water was applied to the surface. Figures 3 are the sketch of the sensor chip and the sequential photographs. From the photographs, it can be seen that the coloration of Ag nanodome arrays returned to the original color soon after the water was removed.

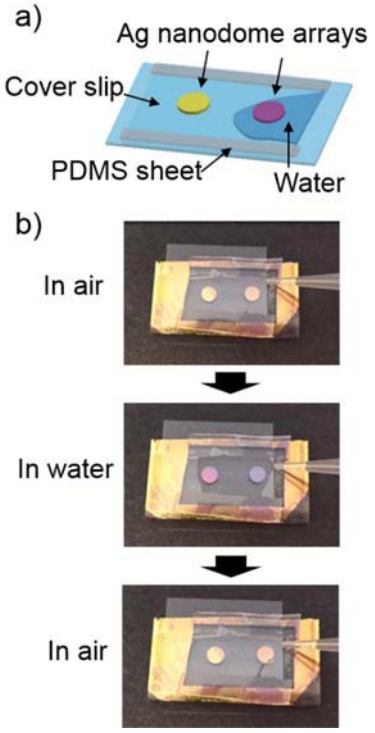

Figure 3 (a) a sketch of the sensor chip consisting of two sensing spots with Ag nanodome arrays (ϕ= 200 nm) and a chamber to apply water. (b) Sequential photographs of the sensor chip upon water apply and removal.

Bulk refractive index sensitivity.

As the fundamental characteristics of Ag and Au nanodome arrays, bulk refractive index sensitivity was investigated. In this experiment, we evaluate the bulk refractive index sensitivity by spectroscopic measurement, namely reflectivity spectra. The wavelength λ_m upon the injection of aqueous solutions sensor responses were recorded as a shift in the resonance

containing ethylene glycol with different mixing ratio (0, 5, 10, 20 and 30 v%). The resonance wavelength was defined by fitting the reflectivity spectra in Fig.2 with a quadratic function with a threshold value. A typical sensor response taken with Ag nanodome array (ϕ= 200 nm) against the injection of the sample solution was shown in Figure 4a. As shown in Fig. 4a, the resonance wavelength immediately shifted and reached plateau when the sample solution was injected. The same experiments were performed for other Ag nanodome arrays (ϕ= 350 and 500 nm) and Au nanodome array (ϕ= 200 nm), and the shifts in resonance wavelength $\Delta\lambda_m$ against the increment of the bulk refractive index ΔRI were plotted in Figure 4b. The measurement was performed more than three times by changing the measurement spots to obtain the standard deviation denoted as error bars. The wavelength dependent refractive indices of the water and ethylene glycol were obtained from the reference.[37] As shown in Fig.4b, the linear relations between the shift in resonance wavelength and the bulk refractive index changes were observed for the all of Ag nanodome arrays. The bulk refractive index sensitivities were obtained as the slopes of the linear fit, and were 162, 497 and 588 nm per refractive index unit (nm/RIU) for Ag nanodome with ϕ= 200, 350 and 500 nm, respectively. The Au nanodome arrays (ϕ= 200 nm) resulted in the better bulk RI sensitivity (264 nm/ RIU) with respect to that of Ag nandome arrays (ϕ= 200 nm). As discussed in the previous section, the bulk refractive index sensitivity improved as the dome diameter increased. Considering the typical bulk RI sensitivities of localized surface plasmon sensors are in the range of 100 to 1000 nm/RIU,[34, 38, 39] our Ag nanodome arrays provide reasonable bulk RI sensitivity. Regarding the metal nanostructures similar to the Ag nanodome arrays, the lower bulk RI sensitivity around 60 to 70 nm/RIU was reported.[40, 41] These reported works were performed using the metal nanostructure created with the smaller dielectric nanospheres (ϕ100 nm). This size effect of Ag nanodome arrays on the refractive index sensitivity agreed with the other studies performed with Au nanorings and Au nanodiscs.[38, 42]

A biosensor for detection of DNA hybridization. To characterize the performance of biosensor using metal nanodome arrays, detection of DNA hybridization was performed. As described in the experimental section, the surface of Ag nanodome arrays was coated with Au thin layer to protect from the oxidation. We would like to note that the optical properties of Ag nanodome arrays were almost retained by deposition of Au layer with thickness around 6 nm. After immobilization of 30 mer single stranded DNA (Rc30) on to the sensor surface, a flow cell made by a PDMS sheet was attached to the sensor surface. The solution containing AuNPs modified with complementary DNA to Rc30 (R30) was flowed over the sensor surface for 40 min by using a peristaltic pump, then rinse with PBS. The reflectivity spectra and photographs of Ag nanodome arrays (ϕ= 200 nm)

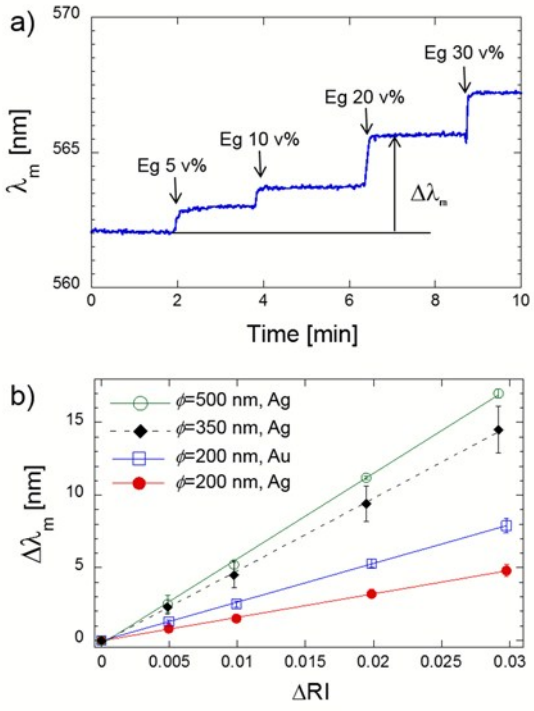

Figure 4 (a) Real time measurement of sensor responses against the injection of ethylene glycol solution with different concentration. (b) Quantitative plot of $\Delta\lambda_m$ against ΔRI.

View Article Online
DOI: 10.1039/C9NA00315K

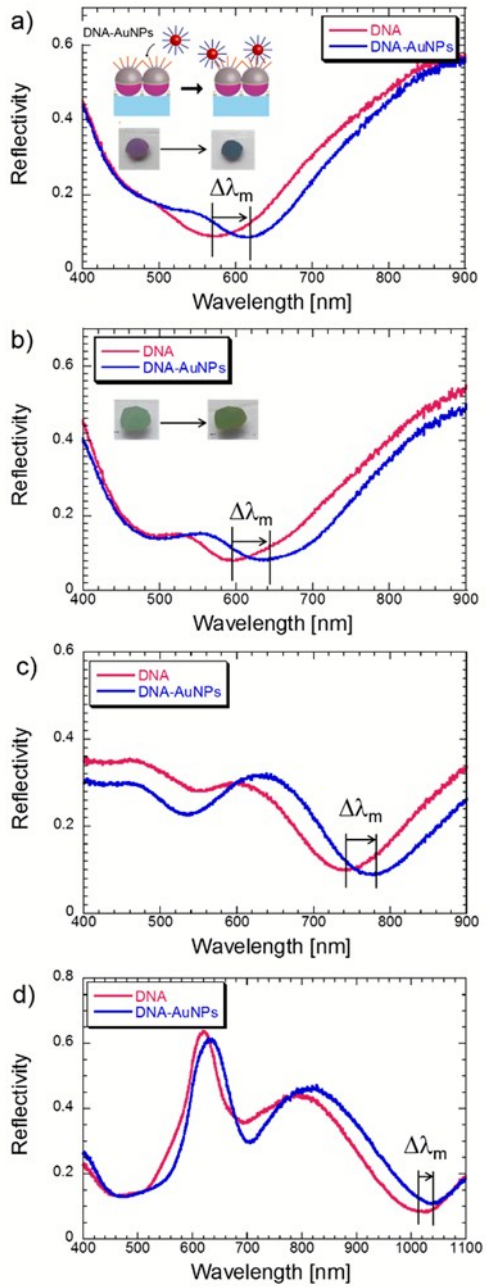

Figure 5 Reflectivity spectra taken before and after the immobilization of DNA-AuNPs. (a) Ag nanodome (ϕ= 200 nm) . (b) Au nanodome (ϕ= 200 nm), (c) Ag nanodome (ϕ= 350 nm) . (d) Ag nanodome (ϕ= 500 nm) .The photographs of sensor spots are inserted in the plot of Ag and Au nanodome (ϕ= 200 nm).

Table 2 Comparison of bulk refractive index sensitivities, and the sensor responses against the binding of DNA-AuNPs of metal nanodome arrays

ϕ [nm]	Metal	Bulk RI Sensitivity [nm/RIU]	Δλm [nm]
200	Ag	162	49 ±9
200	Au	264	35 ±5
350	Ag	497	35 ±3
500	Ag	588	21±3

taken before and after the immobilization of DNA-AuNPs through DNA hybridization were shown in Figure 5a. Immobilization of DNA-AuNPs onto the Ag nanodome array surface induced a large shift in the resonance wavelength of 49 nm accompanied with a dramatic change in coloration from purplish-red to greenish-blue. The initial hue of the sensing spot was 325 deg. The Hue angles shifted to counter clockwise direction in the same manner to bulk refractive index changes, was and the shift amount reached to as high as 130 deg. In the case of Au nanodome array (ϕ= 200 nm), the shift in resonance wavelength supressed to 35 nm, and the change in coloration was not significant with respect to the Ag nanodome array structure. The optical properties of Ag nanodome arrays were mostly retained by depositing the thin Au overlayer. The same experiments were carried out for the other Ag nanodome array (ϕ= 350 and 500 nm), and the reflectivity spectra are shown in Figures 4c-d. The shift amount of resonance wavelength by immobilization of DNA-AuNPs are summarized in Table 2 with the results of bulk RI sensitivity. The shift of resonance wavelength was averaged over the at least three different sensor chips to estimate the standard deviation. Interestingly, the sensor response against the binding of DNA-AuNPs exhibited the contradictory trend from the bulk RI sensitivity. For instance, the maximum shift in resonance wavelength was obtained with Ag nanodome array (ϕ=200 nm), which resulted in the lowest bulk RI sensitivity. Furthermore, only this Ag nanodome array exhibited the color changes due to the immobilization of DNA-AuNPs, even the deformation on reflectivity spectra of Ag nanodome arrays (ϕ=350 and 500 nm) was also observed in the visible wavelength region. Though the local refractive index sensitivity is not always proportional to bulk refractive index sensitivity,[43] we consider that the plasmonic coupling between Ag nanodome array (ϕ=200 nm) and AuNPs induced the higheroptical responses. As shown in reflectivity spectra in Fig.5a, the resonance band of Ag nanodome arrays (ϕ=200 nm) have an overlap with that of LSPR of DNA-AuNPs having an absorption peak at 525 nm. The plasmonic fields may interact with the same manner of a dimer of metal nanoparticles which induce the large shift in resonance wavelength.[44] The distance between the surface of Ag nanodome and AuNPs was estimated to be 14 nm. As the plasmonic filed of metal nanosphere is proportional to their diameter (about 15 nm), we consider plasmonic coupling can be occurred in our experimental systems.

For further experiments, we focus on the Ag nanodome arrays (ϕ=200 nm). In the next experiments, the detection sensitivity of DNA-hybridization using a combination of Ag nanodome arrays (ϕ=200 nm) and DNA-AuNPs was evaluated. Here, we used the patterned sensor chips and a model system to perform multiple measurements at the same time. In particular, the surface coverage of a model target ssDNA was controlled by creating mixed ssDNA monolayers containing Rc30 and T30 on the Ag nanodome arrays surface instead of varying the concentration of target ssDNA.[33,34,45,46] Rc30 has complementary sequence to the ssDNA (R30) anchored to

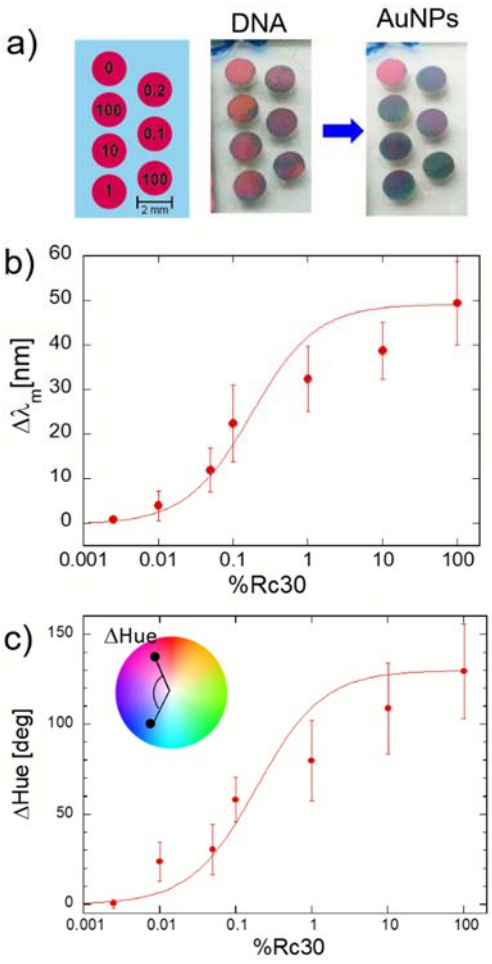

Figure 6 (a) (Left) sketch of the sensing spots, photographs of the sensing spots taken before (middle) and after immobilization of DNA-AuNPs (Right). Quantitative plot of (b) shift amount of resonance wavelength $\Delta\lambda_m$ and (c) shift in hue angle ΔHue against the relative surface coverage of Rc30, %Rc30.

AuNPs, and plays as a model of target DNA. T30 has non-complementary sequence to both Rc30 and R30, therefore immobilization of DNA-AuNPs do not occur. Here, we assume that the probability of immobilization of Rc30 and T30 onto PDA surface via amino-group is equal,[45] and the surface coverage of Rc30 (%Rc30) can be controlled by the mixing ratio of Rc30 and T30 in the solution applying to sensor surface. As shown in Figure 6a, individual sensing spots were modified with Rc30 and T30 with different mixture ratio. In this case, the mixture ratio of Rc30 and T30 was varied from 0:100, 0.1:99.9, 0.2:99.8, 1:99, 10:90, and 100:0 %, indicated as the numbers in the sensing spots in the sketch. To simplified the expression, we described the mixture ratio of Rc30 as its relative surface coverage. The photographs were taken before and after the immobilization of DNA-AuNPs. From the photographs, the visible color changes of the sensing spots were observed depending on the surface coverage of Rc30. Though the color change was not distinguishable for the control spot fully covered with T30, it could be observed for the sensor spot containing Rc30 with the surface coverage down to 0.1 %. As it can be seen in the photograph in Fig. 6a, coloration of Ag nanodome arrays was not perfectly homogeneous. It was caused by the inhomogeneity of the arrangement of Ag nanodome arrays, such as formation of multilayers and disordered structures. Therefore, we reduced the spot size of incident light about 1 mm in diameter to supress the broadening of the reflectivity spectra and to select the sensing areas exhibiting the comparable optical properties. In this experiment, the typical resonance wavelength λ_m and Hue angle of the Ag nanodome arrays were 563 ± 14 nm, and 324 ± 22 deg, respectively. To obtain the quantitative plot, the surface coverage of Rc30 was varied to 0, 0.0025, 0.01, 0.05, 0.1, 1, 10, and 100 %. The experiments were repeated more than four times (n≥4) by using different sensor chips in order to determine the standard deviation of the sensor signals. For spectroscopic measurement, reflectivity spectra were sequentially taken from each sensing spots by moving a sensor chip using a liner stage. The standard deviation σ of resonance wavelength and Hue angle from the same sensing spot was determined to be 0.7 nm and 4.7 deg. After flowing a solution containing DNA-AuNPs and rinsing with PBS, reflectivity spectra were taken again from each sensing spots, then the shifts in resonance wavelength were obtained. The quantitative plot obtained by spectroscopic measurement is shown in Figure 6b. When the sensor surface is covered with control DNA (T30), the $\Delta\lambda_m$ resulted in negligible amount ($\Delta\lambda_m$ = -0.3 nm) which is below the standard deviation σ of the measurement ($\sigma = 0.7$ nm). The clear shift of resonance wavelength ($\Delta\lambda_m$ = 3.9 nm) was observed when the surface coverage of Rc30 reached to 0.01 %. The dramatic change in the $\Delta\lambda_m$ occurred up to 1 %, then the change of $\Delta\lambda_m$ got moderate. For the colorimetric detection, we focused on the shift in hue angles of each sensing spots. The absolute values of shift in hue angle were summarized in Fig. 6c. As shown in Fig. 6c, the quantitative plot obtained by colorimetric method resulted in a good agreement with that taken by spectroscopic method. The change in hue angles can be observed for the surface coverage down to 0.01 %, and the dramatic shift in Hue angle occurs in the range of 0.01 to 1 %. We consider that the quantitative analysis of biomolecules is possible based on colorimetric detection by using the combination of Ag nanodome arrays and AuNPs. The detectable surface coverage of Rc30 was estimated as the intersection of the fitting curve and the three times of the standard deviation describe as 3σ. The determined LOD was 0.03 % of the surface coverage of Rc30. Here, the obtained data may contain relatively large error bar as this experiment was performed under a fluorescent lamp using a smartphone camera without specialized housing. Therefore, we expect that the detection sensitivity can be improved by optimize the setup for colorimetric detection. After performing the end-point measurement to compare the spectroscopic and colorimetric detection, we characterized the detailed sensor responses for the low surface coverage of Rc30 by real time in-situ measurement of resonance wavelength λ_m. In this experiment, the surface coverage of Rc30 was varied to 0, 0.0025, 0.01, 0.05 and 0.1%, and the shift in resonance wavelength $\Delta\lambda$ was recorded as a function of time as shown in Figure 7a. The $\Delta\lambda$ increased after the injection of DNA-AuNPs for the sensor surface containing DNA-Rc30 (%Rc30 ≥ 0.0025), where no

View Article Online
DOI: 10.1039/C9NA00715K

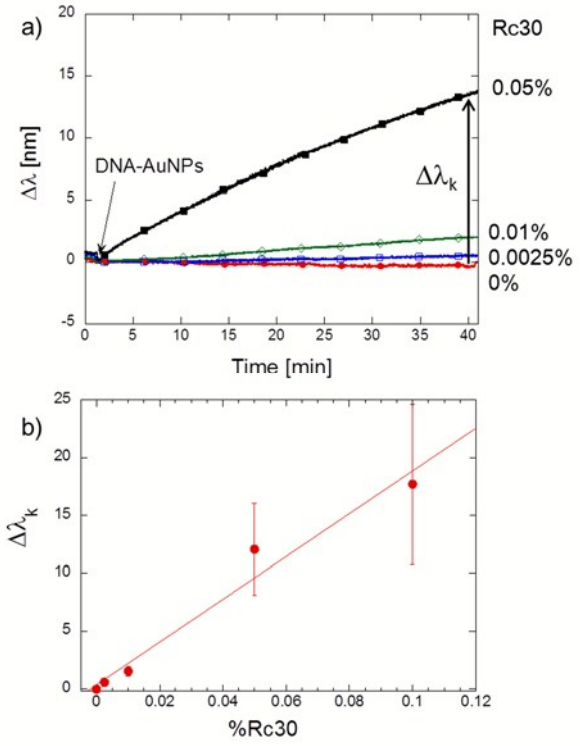

Figure 7 (a) Real time measurement of shift in resonance wavelength $\Delta\lambda$ against the injection of the DNA-AuNPs. (b) Quantitative plot of $\Delta\lambda_k$ against %Rc30.

detectable wavelength shift was observed for the control. After 40 min from the introduction of AuNPs solution, the sensor surface was rinsed with PBS and the shift of the resonance wavelength $\Delta\lambda_k$ was recorded. The quantitative plot of the $\Delta\lambda_k$ as a function of surface coverage Rc30 (%Rc30) is shown in Figure 7b. In this range of surface coverage, the sensor response follows liner relationship. From the standard deviation of the sensor diagram (σ_k=0.04 nm), it is reasonable to consider that the 0.0025 % of %Rc30 resulted in $\Delta\lambda_k$ of 0.58 nm is detectable surface coverage.

Here, we introduce a simple assumption to estimate the detectable concentration of Rc30 from its surface coverage.[33, 34, 45] The surface coverage θ of an ssDNA immobilized on the sensor surface via DNA hybridization can be describe by the Langmuir isotherm equation, using a concentration of target DNA C and the affinity constant of DNA hybridization K_{ads}. When the concentration of DNA C is low enough and the relation $K_{ads} \cdot C \ll 1$ consists, the equation can be described as $\theta = K_{ads} \cdot C$. In our experiment, we assume that the surface coverage of Rc30 is nearly equal to the mixing ratio of Rc30 according to the literature.[45] By using the Langmuir adsorption constant K_{ads} of 10^8 M^{-1},[33] the concentration of ssDNA is estimated to be about 250 fM from the surface coverage θ of Rc30 (0.0025 %). Therefore, we consider that the detection of target DNA at sub pM level is possible by spectroscopic measurement. As the detectable surface coverage of Rc30 was 0.03% by colorimetric detection, the responsible concentration of DNA is about 3 pM. Up to here, we have shown that the presented biosensor scheme based on combination of Ag nanodome arrays (ϕ=200 nm) and DNA-AuNPs can detect DNA hybridization for the relative surface coverage as low as 0.0025 and 0.03 % by spectroscopic method and colorimetric method, respectively. There are several studies reporting the detection sensitivity of DNA hybridization by using the similar samples performed by different optical systems. For instance, the conventional SPR measurement based on the propagating surface plasmons could provide the detectable surface coverage as low as 0.1 %.[33] By using localized surface plasmon biosensor on gold nanoring arrays, the minimum detectable surface coverage was 0.5 %.[34] With respect to these plasmonic biosensors, the Ag nanodome arrays may provide advanced detection sensitivity by much simpler detection scheme. The detection sensitivity of the presented plasmonic biosensor may not reach to that of surface plasmon-enhanced fluorescence (SPF) biosensor on or other ultra-sensitive plasmonic biosensor scheme with much complicated metal structures or optics,[12, 47, 48] the presented biosensor scheme hold a potential for a rapid and sensitive detection of biomolecules without using a specialized equipment.

Conclusions

In this study, we have proposed a sensitive plasmonic biosensor scheme based on colorimetric detection which can perform quantitative detection of biomolecules expressed by hue angles. As the origin of plasmonic coloration, silver and gold nanodome arrays consisting of polystyrene beads layer coated with thin metal films were created over the larger area based on a bottom-up nanofabrication technique. The Ag nanodome arrays exhibited unique coloration varied by the dome size defined by the PS bead diameter. To evaluate the optical properties and sensing performance of Ag nanodome array, both spectroscopic measurements based on reflectivity spectra and colorimetric detections by image analysis of photograph taken by a smartphone camera were carried out. The characterization of bulk refractive index sensitivity revealed that the bulk RI sensitivity improved as the size of nanodome enlarged, and reached to 588 nm/ RIU with Ag nanodome (ϕ= 500 nm). In contrast, the smallest Ag nanodome arrays (ϕ= 200 nm) could provide the highest sensor signals for detection of DNA-hybridization by using DNA modified AuNPs by both spectroscopic and colorimetric measurement. The experimental results implied that the plasmonic coupling between Ag nanodome arrays and DNA-AuNPs plays an important role to generate a large shift in resonance wavelength accompanied with changes in coloration of Ag nanodome arrays. The detection sensitivity for DNA hybridization was evaluated with a model system by controlling a relative surface coverage of the target DNA on the sensor surface. From the plot of sensor signals against the surface coverage of target DNA, it was revealed that the reasonable quantitative measurement can be performed based on colorimetric detection by using a smartphone camera. The detectable surface coverage of target DNA was 0.0025 and 0.03 % by spectroscopic and colorimetric method, respectively, which are corresponding to the concentration sub to few pM level. To the best of our knowledge, this is the first demonstration of colorimetric plasmonic biosensor utilizing

metal nanostructure arrays, enabling sensitive and quantitative detection of biomolecules by hue angle measurement. As the presented biosensor scheme can be versatile for detection of various biomolecules by modifying the sensor surfaces with other bio-recognition element, our future work will include the demonstration of immunoassay for detection of disease related biomolecules such as biomarkers and pathogens.

Conflicts of interest

There are no conflicts to declare.

Acknowledgements

This work was supported by JSPS KAKENHI Grant Numbers, JP15H06766 in Research Activity Start-up, JP16H02092 in Scientific Research (A) and MEXT KAKENHI Grant Number JP17H05273 in Scientific Research on Innovative Areas "Photosynergetics".

Notes and references

1 J. Homola, *Chem. Rev.*, 2008, **108**, 462.
2 M. Bauch, K. Toma, M. Toma, Q. Zhang and J. Dostalek, *Plasmonics*, 2014, **9**, 781.
3 M. E. Stewart, C. R. Anderton, L. B. Thompson, J. Maria, S. K. Gray, J. A. Rogers and R. G. Nuzzo, *Chem. Rev.*, 2008, **108**, 494.
4 B. Liedberg, C. Nylander and I. Lundstrom, *Biosens. Bioelectron.*, 1995, **10**, R1.
5 O. Tokel, F. Inci and U. Demirci, *Chem. Rev.*, 2014, **114**, 5728.
6 A. G. Brolo, *Nat. Photonics*, 2012, **6**, 709.
7 X. H. Wang, T. W. Chang, G. H. Lin, M. R. Gartia and G. L. Liu, *Anal. Chem.*, 2017, **89**, 611.
8 K. Toma, M. Vala, P. Adam, J. Homola, W. Knoll and J. Dostalek, *Opt. Express*, 2013, **21**, 10121.
9 A. Prasad, J. Choi, Z. Jia, S. Park and M. R. Gartia, *Biosens. Bioelectron.*, 2019, **130**, 185.
10 J. L. Zhang, I. Khan, Q. W. Zhang, X. H. Liu, J. Dostalek, B. Liedberg and Y. Wang, *Biosens. Bioelectron.*, 2018, **99**, 312.
11 C. Lertvachirapaiboon, A. Baba, K. Shinbo and K. Kato, *Anal. Methods*, 2018, **10**, 4732.
12 M. Toma, S. Izumi and K. Tawa, *Analyst*, 2018, **143**, 858.
13 K. Tawa, M. Umetsu, T. Hattori and I. Kumagai, *Anal. Chem.*, 2011, **83**, 5944.
14 A. Ricciardi, A. Crescitelli, P. Vaiano, G. Quero, M. Consales, M. Pisco, E. Esposito and A. Cusano, *Analyst*, 2015, **140**, 8068.
15 A. E. Cetin, A. F. Coskun, B. C. Galarreta, M. Huang, D. Herman, A. Ozcan and H. Altug, *LIGHT-SCI APPL*, 2014, **3,** e122.
16 A. Leitis, A. Tittl, M. Liu, B. H. Lee, M. B. Gu, Y. S. Kivshar and H. Altug, Science Advances, 2019, 5, eaaw2871.
17 Y. Liu, Q. Liu, S. Chen, F. Cheng, H. Wang and W. Peng, Scientific Reports, 2015, 5, 1.
18 H. Guner, E. Ozgur, G. Kokturk, M. Celik, E. Esen, A. E. Topal, S. Ayas, Y. Uludag, C. Elbuken and A. Dana, Sensors and Actuators, B: Chemical, 2017, 239, 571.
19 L. H. Tang and J. H. Li, *Acs Sensors*, 2017, **2**, 857.
20 P. Chen, X. Liu, G. Goyal, T. Nhung Thi, J. C. S. Ho, Y. Wang, D. Aili and B. Liedberg, *Anal. Chem.*, 2018, **90**, 4916.
21 K. Kumar, H. G. Duan, R. S. Hegde, S. C. W. Koh, J. N. Wei and J. K. W. Yang, *Nat. Nanotechnol.*, 2012, **7**, 557.
22 R. Mudachathi and T. Tanaka, *Sci. Rep.*, 2017, **7**, 1199.
23 X. L. Zhu, C. Vannahme, E. Hojlund-Nielsen, N. A. Mortensen and A. Kristensen, *Nat. Nanotechnol.*, 2016, **11**, 325.
24 L. Wang, R. J. H. Ng, S. Safari Dinachali, M. Jalali, Y. Yu and J. K. W. Yang, *ACS Photonics*, 2016, **3**, 627. View Article Online DOI: 10.1039/C9NA00315K
25 S. Shinohara, D. Tanaka, K. Okamoto and K. Tamada, *Phys. Chem. Chem. Phys.*, 2015, **17**, 18606.
26 M. R. Gartia, A. Hsiao, A. Pokhriyal, S. Seo, G. Kulsharova, B. T. Cunningham, T. C. Bond and G. L. Liu, *Adv. Opt. Mater.*, 2013, **1**, 68.
27 I. Misbah, F. S. Zhao and W. C. Shih, *ACS Appl. Mater. Interfaces*, 2019, **11**, 2273.
28 Z. Yi, G. Niu, J. Luo, X. Kang, W. Yao, W. Zhang, Y. Yi, Y. Yi, X. Ye, T. Duan and Y. Tang, *Sci. Rep.*, 2016, **6**, 32314.
29 K. Sugawa, T. Tamura, H. Tahara, D. Yamaguchi, T. Akiyama, J. Otsuki, Y. Kusaka, N. Fukuda and H. Ushijima, *Acs Nano*, 2013, **7**, 9997.
30 T. Endo, K. Kerman, N. Nagatani, H. M. Hiepa, D. K. Kim, Y. Yonezawa, K. Nakano and E. Tamiya, *Anal. Chem.*, 2006, **78**, 6465.
31 M. Toma, G. Loget and R. M. Corn, *ACS Appl. Mater. Interfaces*, 2014, **6**, 11110.
32 A. R. Halpern and R. M. Corn, *ACS Nano*, 2013, **7**, 1755.
33 J. B. Wood, M. W. Szyndler, A. R. Halpern, K. Cho and R. M. Corn, *Langmuir*, 2013, **29**, 10868.
34 M. Toma, K. Cho, J. B. Wood and R. M. Corn, *Plasmonics*, 2014, **9**, 765.
35 A. R. Smith, *SIGGRAPH Comput. Graph.*, 1978, **12**, 12.
36 C. Farcau and S. Astilean, *Appl. Phys. Lett.*, 2009, **95,** 193110.
37 H. El-Kashef, *Physica B*, 2000, **279**, 295.
38 E. M. Larsson, J. Alegret, M. Kall and D. S. Sutherland, *Nano Lett.*, 2007, **7**, 1256.
39 K. M. Mayer and J. H. Hafner, *Chem. Rev.*, 2011, **111**, 3828.
40 M. Himmelhaus and H. Takei, *Sens. Actuators, B*, 2000, **63**, 24.
41 D. K. Kim, S. M. Yoo, T. J. Park, H. Yoshikawa, E. Tamiya, J. Y. Park and S. Y. Lee, *Anal. Chem.*, 2011, **83**, 6215.
42 P. Hanarp, M. Kall and D. S. Sutherland, *J. Phys. Chem. B*, 2003, **107**, 5768.
43 M. Piliarik, H. Sipova, P. Kvasnicka, N. Galler, J. R. Krenn and J. Homola, *Opt. Express*, 2012, **20**, 672.
44 N. J. Halas, S. Lal, W. S. Chang, S. Link and P. Nordlander, *Chem. Rev.*, 2011, **111**, 3913.
45 Y. L. Chen, A. Nguyen, L. F. Niu and R. M. Corn, *Langmuir*, 2009, **25**, 5054.
46 A. R. Halpern, J. B. Wood, Y. Wang and R. M. Corn, *Acs Nano*, 2014, **8**, 1022.
47 J. Dostalek and W. Knoll, Biointerphases, 2008, **3**, FD12.
48 K. Tawa, F. Kondo, C. Sasakawa, K. Nagae, Y. Nakamura, A. Nozaki and T. Kaya, *Anal. Chem.*, 2015, **87**, 3871.

View Article Online
DOI: 10.1039/C9NA00315K

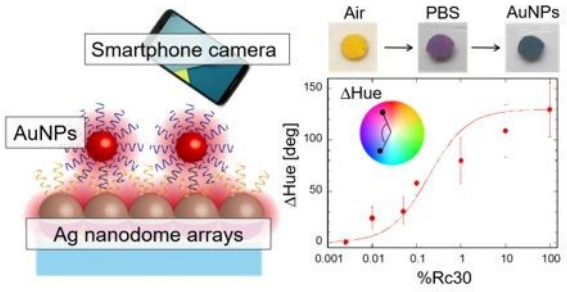

Plasmonic coloration from silver nanodome arrays is successfully implemented into a smartphone-based biosensor enabling sensitive and quantitative detection of biomolecules.